Int J Thermophys (2014) 35:865–889
DOI 10.1007/s10765-014-1680-7

An Improved Computational Method for the Calculation of Mixture Liquid–Vapor Critical Points

Panagiotis Dimitrakopoulos · Wenlong Jia · Changjun Li

Received: 11 February 2014 / Accepted: 28 June 2014 / Published online: 20 July 2014

Abstract Knowledge of critical points is important to determine the phase behavior of a mixture. This work proposes a reliable and accurate method in order to locate the liquid–vapor critical point of a given mixture. The theoretical model is developed from the rigorous definition of critical points, based on the SRK equation of state (SRK EoS) or alternatively, on the PR EoS. In order to solve the resulting system of $C + 2$ nonlinear equations, an improved method is introduced into an existing Newton–Raphson algorithm, which can calculate all the variables simultaneously in each iteration step. The improvements mainly focus on the derivatives of the Jacobian matrix, on the convergence criteria, and on the damping coefficient. As a result, all equations and related conditions required for the computation of the scheme are illustrated in this paper. Finally, experimental data for the critical points of 44 mixtures are adopted in order to validate the method. For the SRK EoS, average absolute errors of the predicted critical-pressure and critical-temperature values are 123.82 kPa and 3.11 K, respectively, whereas the commercial software package Calsep PVTSIM's prediction errors are 131.02 kPa and 3.24 K. For the PR EoS, the two above mentioned average absolute errors are 129.32 kPa and 2.45 K, while the PVTSIM's errors are 137.24 kPa and 2.55 K, respectively.

P. Dimitrakopoulos (✉)
Graduate of the Technical University of Berlin, 10623 Berlin, Germany
e-mail: dimitrakopoulos@gmx.de

W. Jia (✉) · C. Li
School of Petroleum Engineering, Southwest Petroleum University, Chengdu 610500, China
e-mail: jiawenlongswpu@hotmail.com

C. Li
CNPC Key Laboratory of Oil & Gas Storage and Transportation, Southwest Petroleum University, Chengdu 610500, China

Keywords Critical point · Damped Newton–Raphson method · Equation of state · Hydrocarbon mixture · Vapor–liquid equilibrium

1 Introduction

The liquid–vapor critical point is defined as the intersection point of the dew-point curve and bubble-point curve in a pressure–temperature phase diagram. At the critical point, the properties of the liquid and vapor phases converge, resulting in two phases which have the same thermodynamic properties [1]. Knowledge of the critical point is useful for mixture processing and transportation. The critical point can help to specify the phase of a mixture, and to determine operational pressures and temperatures in pipelines and process equipment. For example, liquid petroleum gas (LPG) is a multicomponent mixture mainly composed of ethane, propane, butane, and heavier hydrocarbons, which is usually transported in pipelines. In order to ensure LPG remains in the liquid phase, the pressure should remain above the critical pressure [2,3]. Similarly, the pressure and temperature in a supercritical CO_2 pipeline also should be in the region beyond the critical point [4]. Besides, the liquid–vapor critical point is also a key parameter to determine the gas reservoir type [5]. Additionally, knowledge of the true critical pressure and temperature values contributes directly to improvement of calculation results which are based on the principle of corresponding states and EoS models [6].

There are several ways to determine the liquid–vapor critical point of a mixture, such as experiments, empirical correlations, and theoretical models. The theoretical approach is one of the most important methods in determining the critical point. One approach in order to find the critical points is to calculate the entire phase envelope, such as described in Michelsen's work [7]. In the past 40 years, great progress has been made in generating phase envelopes. Recently, Ortiz-Vega et al. [8], Venkatarathnam [9], and many other researchers have been working on the accuracy and high-speed phase envelope generation method. However, if only the critical point is required, the generation of the phase envelope should be avoided, since it is associated with complicated computations of bubble points and dew points.

In order to locate the critical point directly, Heidemann and Khalil [10] proposed a method to calculate critical points of multicomponent mixtures, first based on their rigorous definition, which consists of two equations of partial derivatives of the molar Helmholtz energy that must vanish at the critical point. Heidemann and Khalil employed two nested single-variable iteration loops and the Newton–Raphson method to solve the model. The independent variables are the critical temperature and critical molar volume. First, the critical temperature is calculated by holding the critical molar volume constant in the inner iteration loop. Second, the critical molar volume is calculated by the external iteration loop [11]. Wang et al. [12] used the homotopy continuation technique for the calculation of critical points in binary mixtures. Stradi et al. [13] transformed the Heidemann and Khalil model into a set of equations, in which the variables are the critical volume, critical temperature, and perturbations in the component compositions. The interval Newton analysis method is adopted to solve the model. Also, many researchers have treated the solution of the model as

a global optimization problem. As a result, some algorithms, such as the simulated annealing algorithm [14], differential evolution algorithm, and stochastic optimization methods [15] have been used. Although the optimization methods have shown good performance in solving the model, some adjustable parameters should be determined carefully to ensure the robustness of the algorithms [14].

Based on the theoretical achievements regarding both the phase envelope generation, and critical-point calculation method, some commercial software tools have been developed, such as the NIST REFPROP, GERG [9], Aspen HYSYS, and Calsep PVTSIM [16].

Although many publications deal with the calculation of critical points, and software tools can help us locate the critical points, only a little work can be found that gives detailed information about the implementation of such an algorithm. Recently, Jia et al. [11] proposed a damped Newton–Raphson method in order to solve the Heidemann and Khalil model in each iteration step. He also illustrated some details about programming the critical points. However, the convergence criteria shown in [11] were not accurate enough and the value for the damping coefficient was fixed, thus reducing the accuracy and robustness of the damped Newton–Raphson method.

This paper is based on Stradi's model with some very small corrections, and on the PR and SRK equations of state (PR EoS and SRK EoS) to calculate the liquid–vapor critical points of multicomponent mixtures, but the proposed method for the solution of the equations in this paper differs from that in Stradi's publication. The solution method is mainly based on Jia's method, whereas the recommendations for the choice of the adjustable damping coefficient and for the convergence criteria have been improved. Besides, the derivatives appearing in the Jacobian matrix are specified in detail. As a result, all equations and related conditions required for the computation of the scheme are illustrated in this paper, also providing good guidelines for the reproduction of the computational work shown in this publication. Furthermore, the results show that the improved computational method has a satisfactory accuracy. The improved method can be used to compute liquid–vapor critical points of multicomponent mixtures in good agreement with reality.

2 Critical-Point Model

Gibbs presented a rigorous definition of critical points based on phase stability theory. But his method becomes very complex for multicomponent systems. Heidemann and Khalil used the Helmholtz energy A to replace the Gibbs free energy and expanded the Helmholtz energy by applying a Taylor series expansion. Then, the critical-point model can be written as follows [13]:

$$\sum_{j=1}^{C}\left(\frac{\partial^2 A}{\partial n_i \partial n_j}\right)_{T_c,v_c}\Delta n_j = 0, \tag{1}$$

$$\sum_{m=1}^{C}\sum_{j=1}^{C}\sum_{i=1}^{C}\left(\frac{\partial^3 A}{\partial n_m \partial n_i \partial n_j}\right)_{T_c,v_c}\Delta n_i \Delta n_j \Delta n_m = 0, \tag{2}$$

where C is the total number of mixture components, n is the number of moles, Δn is the change in number of moles, T_c is the critical temperature, and v_c is the critical molar volume; subscripts i, j, m represent the ith, jth, and mth component, respectively. Some authors use a double summation in Eq. 1, but the single summation shown in Eq. 1 and which is also shown in [13], is directly the right equation, from which an equation with a double summation can be derived, because $i = 1, 2, \ldots, C$. In general, the non-zero changes in the numbers of moles are considered in Eqs. 1 and 2.

Equations 1 and 2 can also be written with respect to fugacity as follows:

$$\sum_{j=1}^{C} RT \left(\frac{\partial \left(\ln f_{gi} \right)}{\partial n_j} \right)_{T_c, v_c} \Delta n_j = 0, \tag{3}$$

$$\sum_{m=1}^{C} \sum_{j=1}^{C} \sum_{i=1}^{C} RT \left(\frac{\partial^2 \left(\ln f_{gi} \right)}{\partial n_j \partial n_m} \right)_{T_c, v_c} \Delta n_i \Delta n_j \Delta n_m = 0, \tag{4}$$

where R is the gas constant and f_{gi} is the fugacity of component i, which can be calculated from the PR and SRK EoS.

Based on the PR and SRK EoS, the critical-point calculation model shown by Eqs. 3 and 4 can be transformed into Eqs. 5 and 6. Some small mistakes with regard to the derivation of the model which appear in [11] and [13] are corrected in this work. Equation 5 follows from Eqs. 1 and 3, while Eq. 6 is equivalent to Eqs. 2 and 4:

$$\frac{RT_c}{n} \left(\frac{\Delta n_i}{y_i} + F_1 \left(\beta_i \bar{N} + \bar{\beta} \right) + \beta_i F_1^2 \bar{\beta} \right) + \frac{a}{bn} \left(\beta_i \bar{\beta} F_3 - \frac{F_5}{a} \sum_{j=1}^{C} \left(a_{ij} \Delta n_j \right) + F_6 \left(\beta_i \bar{\beta} - \alpha_i \bar{\beta} - \bar{\alpha} \beta_i \right) \right) = 0, \tag{5}$$

$$\frac{RT_c}{n^2} \left(- \sum_{i=1}^{C} \frac{\Delta n_i^3}{y_i^2} + 3 \bar{N} \left(\bar{\beta} F_1 \right)^2 + 2 \left(F_1 \bar{\beta} \right)^3 \right) + \frac{a}{n^2 b} \left(3 \bar{\beta}^2 \left(2 \bar{\alpha} - \bar{\beta} \right) \left(F_3 + F_6 \right) - 2 \bar{\beta}^3 F_4 - 3 \bar{\beta} \bar{a} F_6 \right) = 0, \tag{6}$$

where $i = 1, 2, \ldots, C$. The auxiliary factors $F_1, F_2, F_3, F_4, F_5, F_6$ and the parameters $a, b, \beta_i, \bar{N}, \bar{\beta}, a_{ij}, \alpha_i, \bar{\alpha}$, and $\bar{a}$ are related to the selected EoS (PR or SRK). The mole fraction of component i has the symbol y_i. The definitions of these parameters and of n are listed in Appendix 1. Note that Eqs. 5 and 6 are implicit in the critical molar volume.

Also note that the auxiliary factor F_2 does not appear in Eqs. 5 and 6. F_2 was just defined and used in the derivation procedure in order to determine other auxiliary factors, and is correctly not used in the above equations.

The changes in the numbers of moles have to satisfy Eq. 7. This equation is valid for $\Delta \boldsymbol{n}$ as a normalized vector and assures that its components are in general non-zero [7,13]:

$$\sum_{i=1}^{C} \Delta n_i^2 - 1 = 0. \tag{7}$$

The square root belonging to the vector normalization has been ignored, as the square root of 1 is equal to 1. Thus, Eq. 7 is, as already mentioned, valid for a normalized $\Delta \boldsymbol{n}$-vector.

Finally, the critical-point computation model is based on Eqs. 5–7. As Eq. 5 represents C equations, there are finally $C+2$ equations and $C+2$ variables in the model: Those variables are: T_c, v_c, and Δn_i (where $i = 1, 2, \ldots, C$). By solving the model as shown in the next section, the critical temperature T_c, critical molar volume v_c, and the perturbations regarding the number of moles of each component Δn_i can be obtained. Then, the critical pressure P_c can easily be computed by substituting the already calculated variables into the selected EoS [11].

3 Model Solution

3.1 Damped Newton–Raphson Method

The critical-point calculation model is a system of nonlinear equations. Thus, all the variables in the model can be solved by using the Newton–Raphson method, and as shown later, by slightly modifying it with the introduction of a damping coefficient. We introduce the following definitions. The left side of Eq. 5 is defined as f_{1i}, where $i = 1$ to C, the left side of Eq. 6 is defined as f_2, and the left side of Eq. 7 is defined as f_3.

$$\begin{aligned} f_{1i} = {} & \frac{RT_c}{n}\left(\frac{\Delta n_i}{y_i} + F_1\left(\beta_i \bar{N} + \bar{\beta}\right) + \beta_i F_1^2 \bar{\beta}\right) \\ & + \frac{a}{bn}\left(\beta_i \bar{\beta} F_3 - \frac{F_5}{a}\sum_{j=1}^{C}\left(a_{ij}\Delta n_j\right) + F_6\left(\beta_i \bar{\beta} - \alpha_i \bar{\beta} - \bar{\alpha}\beta_i\right)\right) \\ & i = 1, 2, \ldots, C, \end{aligned} \tag{8}$$

$$\begin{aligned} f_2 = {} & \frac{RT_c}{n^2}\left(-\sum_{i=1}^{C}\frac{\Delta n_i^3}{y_i^2} + 3\bar{N}\left(\bar{\beta}F_1\right)^2 + 2\left(F_1\bar{\beta}\right)^3\right) \\ & + \frac{a}{n^2 b}\left(3\bar{\beta}^2\left(2\bar{\alpha} - \bar{\beta}\right)\left(F_3 + F_6\right) - 2\bar{\beta}^3 F_4 - 3\bar{\beta}\bar{a}F_6\right), \end{aligned} \tag{9}$$

$$f_3 = \sum_{i=1}^{C} \Delta n_i^2 - 1. \tag{10}$$

In Eqs. 8–10, the variables are T_c, v_c, and Δn_i. Thus, the Newton–Raphson iteration format of the model is written as shown in [11]

$$\begin{bmatrix} \frac{\partial f_{11}}{\partial T_c} & \frac{\partial f_{11}}{\partial v_c} & \frac{\partial f_{11}}{\partial \Delta n_1} & \cdots & \frac{\partial f_{11}}{\partial \Delta n_C} \\ \frac{\partial f_{12}}{\partial T_c} & \frac{\partial f_{12}}{\partial v_c} & \frac{\partial f_{12}}{\partial \Delta n_1} & \cdots & \frac{\partial f_{12}}{\partial \Delta n_C} \\ & & \cdots & & \\ \frac{\partial f_{1C}}{\partial T_c} & \frac{\partial f_{1C}}{\partial v_c} & \frac{\partial f_{1C}}{\partial \Delta n_1} & \cdots & \frac{\partial f_{1C}}{\partial \Delta n_C} \\ \frac{\partial f_2}{\partial T_c} & \frac{\partial f_2}{\partial v_c} & \frac{\partial f_2}{\partial \Delta n_1} & \cdots & \frac{\partial f_2}{\partial \Delta n_C} \\ 0 & 0 & \frac{\partial f_3}{\partial \Delta n_1} & \cdots & \frac{\partial f_3}{\partial \Delta n_C} \end{bmatrix} \begin{bmatrix} \Delta T_c \\ \Delta v_c \\ \Delta\Delta n_1 \\ \Delta\Delta n_2 \\ \\ \vdots \\ \\ \\ \Delta\Delta n_C \end{bmatrix} = - \begin{bmatrix} f_{11}\left(\boldsymbol{x}^k\right) \\ f_{12}\left(\boldsymbol{x}^k\right) \\ \\ \vdots \\ \\ f_{1C}\left(\boldsymbol{x}^k\right) \\ f_2\left(\boldsymbol{x}^k\right) \\ f_3\left(\boldsymbol{x}^k\right) \end{bmatrix} \tag{11}$$

where ΔT_c, Δv_c, and $\Delta\Delta n_i$ are the correction terms for the critical temperature, critical molar volume, and for the change of the number of moles of the mixture's ith component, respectively; superscript k represents the number of the iteration step and is not an exponent.

Equation 11 can also be written as follows:

$$\boldsymbol{J}\,\Delta\mathbf{x} = -\boldsymbol{F}\,(\mathbf{x})\,, \tag{12}$$

where $\boldsymbol{J}$ is the Jacobian matrix, consisting of the shown partial derivatives of the functions f_{1i}, f_2, and f_3. Those derivatives can either be obtained from a numerical or from an analytical method. The equations for the calculation of those partial derivatives are listed in Appendices 1 and 2. In order to reduce computer calculation time, it is recommended to use the analytically obtained partial derivatives—shown in Appendix 2. $\Delta\boldsymbol{x}$ is the correction term as a vector, $\boldsymbol{x}$ is the vector which contains the variables (critical temperature, critical molar volume, and changes in component mole numbers), and $\boldsymbol{F}$ is the vector which contains the f-values at the actual iteration step:

$$\Delta\boldsymbol{x} = (\Delta T_c, \Delta v_c, \Delta\Delta n_1, \ldots, \Delta\Delta n_C)^{\mathrm{T}}\,, \tag{13}$$

$$\boldsymbol{x} = (T_c, v_c, \Delta n_1, \ldots, \Delta n_C)^{\mathrm{T}}\,, \tag{14}$$

$$\boldsymbol{F} = (f_{11}, f_{12}, \ldots, f_{1C}, f_2, f_3)^{\mathrm{T}}\,. \tag{15}$$

For the calculation of the correction term from Eq. 12, use of the Gaussian elimination method is recommended [17]. The superscript T appearing in Eqs. 13–15 represents transposed elements.

In general, the convergence of the Newton–Raphson algorithm depends on the initial values of the variables and the convergence criteria. The initial values can be set by Eqs. 16–18 [11].

Initial value of the critical molar volume:

$$v_{c0} = \sum_{i=1}^{C} (y_i v_{ci}). \tag{16}$$

Initial value of the critical temperature:

$$T_{c0} = 3 \sum_{i=1}^{C} (y_i T_{ci}). \tag{17}$$

Initial value of the change regarding the number of moles of each component:

$$\Delta n_{i\,0} = y_i^{2/3}, \tag{18}$$

where $y_i = n_i/n$, as the initial or specified mole fraction of component i, T_{ci} is the critical temperature of component i, and finally, v_{ci} is the critical molar volume of component i.

The convergence criteria with regard to corrections in the critical temperature, critical molar volume, and changes of component molar amounts, are important with respect to the accuracy of the results. This paper adopts stricter convergence criteria than those used in [11]. The improved convergence criteria are given by

$$|\Delta T_c| < 0.0001\ \mathrm{K}, \tag{19}$$

$$|\Delta v_c| < 10^{-8}\ \mathrm{m^3 \cdot mol^{-1}}, \tag{20}$$

$$|\Delta \Delta n_i| < 0.0001\ \mathrm{mol}\ (i = 1, 2, \ldots, C)\,. \tag{21}$$

Additionally, and in order to examine if the system of the $C+2$ nonlinear equations is really solved, the vector $\boldsymbol{F}$ shall be checked, because $\boldsymbol{F}$ is expected to be approximately equal to the zero vector at the last iteration step.

Based on the classical (not-damped) Newton–Raphson algorithm, the equation for the solution of the critical-point model can be written as

$$\boldsymbol{x}^{k+1} = \boldsymbol{x}^k + \Delta \boldsymbol{x}^k. \tag{22}$$

For a system of linear equations, Eq. 22 would lead to the exact solution. However, the critical-point computation model consists of a system of nonlinear equations. The classical Newton–Raphson method exhibits a tendency to overestimate the correction term $\Delta \boldsymbol{x}^k$. This often disables the convergence of the algorithm [18]. In other words, even if the above initial values and convergence criteria are used in the algorithm, the classical solution method (as the classical Newton–Raphson method) is not reliable enough to predict critical points of multicomponent mixtures. In order to solve this problem, we used a damping function D to adjust the update of $\Delta \boldsymbol{x}^k$ in Eq. 22, so that the correction terms could remain in the convergence region [19]. The new, damped equation was then expressed by [20]

$$\boldsymbol{x}^{k+1} = \boldsymbol{x}^k + D \Delta \boldsymbol{x}^k. \tag{23}$$

In Eqs. 22 and 23, superscript k represents the number of the iteration step and is not an exponent. The reasons for the use of Eq. 23 will be explained in the following section.

3.2 Discussion About the Damping Function and Damping Coefficient

As stated earlier, a function or coefficient had to be found in order to achieve efficient damping with regard to the Newton–Raphson method, as the classical (or not-damped) method was often not able to converge to the desired liquid–vapor critical point of a given mixture. The expression "efficient damping" means ideally balanced damping, which first enables the effect of damping by making the numerical step length smaller, and second avoids long computer calculation times by means of excessive damping (overdamping). In this case of an extremely high degree of damping, the numerical step length would be so small, that a very long time would be necessary to reach the solution, or in other words to converge [21].

Always depending on the initial values for the system variables T_c, v_c, and Δn_i, different damping coefficients have been used. Equation 23 [20] fulfilled all necessary damping requirements and was able to lead back to the classical (not-damped) Newton–Raphson method for $D = 1$, or in other words if $Q = 0$, where Q represents the damping coefficient. In Eq. 23, D is defined as follows:

$$D = \frac{1}{1 + Q \exp(-0.5k)}. \tag{24}$$

It should be noted that in general, D and $\Delta \boldsymbol{x}$ have to be calculated at any iteration step k.

Obviously, after a finite number of iteration steps, the damping function D shown in Eq. 23 shall approximately be unity, in order to approximate Eq. 22, thus enabling the convergence of the algorithm without unnecessarily providing any further damping, which in this case would just delay the reaching of the desired convergence [20].

In general, from the used values $Q \geq 0$ follows that $0 < D \leq 1$. Additionally, for $Q > 0$ is the limit of D for a number of k iteration steps, with $k \to \infty$, approximately equal to 1. This is partially illustrated in Fig. 1, based on a random value of Q. Please note that an inflection point always appears as shown in Fig. 1, corresponding to any $Q > 0$. For a given damping function D (Eq. 24), the position of this inflection point depends only on the Q-value used.

In order to illustrate the relationship between Q and the minimum number of iteration steps which are needed in order to reach $D \geq 0.999$ (in other words $D \approx 1$), Fig. 2 is shown.

Higher Q-values have not been shown on Fig. 2, because as mentioned earlier, they are just causing an undesirable overdamping: That has also been confirmed in practice, and especially, based on computer calculations.

Obviously, as the value of Q increases, even more iteration steps are needed in order to reach $D \geq 0.999$, and thus longer calculations are needed until convergence can be reached. On the other hand, as the value of Q decreases, the damping effect gets

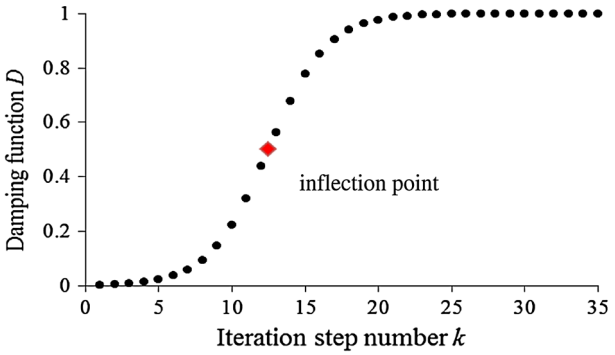

Fig. 1 Damping function D versus iteration step number k

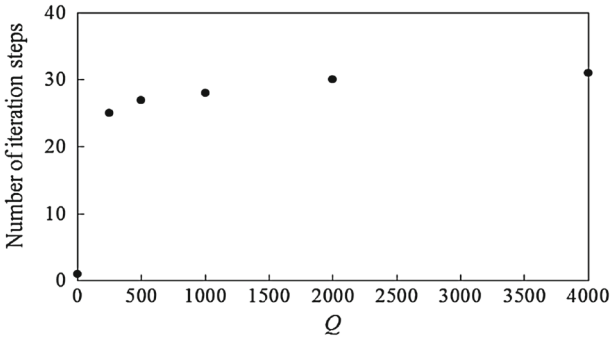

Fig. 2 Minimum number of iteration steps needed to reach $D \geq 0.999$ versus Q

lessened or even vanishes, if $Q = 0$. Thus, a value of Q had to be found, which should be high enough to lead to efficient damping, and at the same time, the value should be as low as possible, in order to reduce the computer calculation time by reaching $D \approx 1$ as quickly as possible.

According to [22], numerical experiments are in general needed in order to estimate damping coefficients. Those numerical experiments were accomplished by using different values for the damping coefficient Q and by always trying to find the minimum Q-value, with which computational convergence could be reached, in order to minimize the computer calculation time. Thus, based on a numerical study with regard to different mixtures and by giving attention to the number of needed iteration steps until convergence was reached, the following was observed: The numerical calculations for the studied mixtures converged when the inflection point, as shown in Fig. 1, corresponded to a mean value of approximately 12.5 iteration steps (at $k = 12.5$).

Thus, we can calculate a mean Q-value, corresponding to $k = 12.5$. This task requires the first and second derivatives of D with respect to k. From Eq. 24 we obtain

$$\frac{\mathrm{d}D}{\mathrm{d}k} = \frac{1}{2} Q D^2 \exp(-0.5k) \tag{25}$$

and

$$\frac{\mathrm{d}^2 D}{\mathrm{d}k^2} = \left(\frac{\mathrm{d}D}{\mathrm{d}k} - \frac{1}{4}D\right) Q D \exp(-0.5k). \tag{26}$$

The condition for the inflection point is mathematically described by

$$\frac{\mathrm{d}^2 D}{\mathrm{d}k^2} = 0. \tag{27}$$

In general, Q and D are both positive. The exponential term is also positive. Thus, after substituting Eq. 26 into Eq. 27, it follows that

$$\frac{\mathrm{d}D}{\mathrm{d}k} - \frac{1}{4}D = 0. \tag{28}$$

By substituting Eqs. 24 and 25 into Eq. 28 and then solving for Q, for a given k, the final equation which leads to the corresponding value of Q at the inflection point is $Q = 1/\exp(-0.5k)$. From that last equation, it follows that $Q \approx 518$ with $k = 12.5$.

Thus, according to a numerical study with regard to a large number of mixtures which cannot be further discussed in this paper, the above mentioned optimum Q-value ($Q = 518$) was confirmed. In general, we suggest the use of this Q-value as the standard initial value to be used in Eq. 24. Only for binary mixtures is $Q = 0$ the recommended initial value for the damping coefficient, as the calculations for the critical points of those mixtures, in most cases, do not require any damping to converge.

The big advantage of the Newton–Raphson method, compared to other iterative methods, is the high speed at which convergence can be reached, especially when the initial values for the variables are in the vicinity of the roots [21]. A disadvantage of this method, for example, compared to the bisection method, is the fact that in such cases, it is very difficult to reliably prove the non-existence of a mathematical root, or in this case, of a liquid–vapor critical point. If by using the above mentioned initial Q-value no critical point could be located with this method, other Q-values should be used, as shown in Fig. 2, beginning with $Q = 0$. As already mentioned and confirmed by computer calculations, higher Q-values would just lead to undesirable and unnecessarily time-consuming overdamping. By using different Q-values in order to reach convergence, it is recommended to equip the computer program with an error handling routine [17], which, for example, would enable the recalculation based on the algorithm with the next Q-value without interrupting the calculation procedure in order to show an error message.

As shown in [13], interval methods represent a reliable technique for the calculation of critical points, but require a relatively long time to locate a critical point. Based on the bisection method, it is theoretically possible to prove the non-existence of a liquid–vapor critical point of a mixture, by subdividing the whole interval, in which possible roots could exist, into n subintervals, where n is a large number, and then, by showing that no sign changes of the corresponding function take place at the boundaries of those intervals. Unfortunately, the computer calculation time would in this case tend to be relatively long.

Table 1 Properties of pure components

Component	P_c (kPa)	T_c (K)	ω (−)	v_c ($m^3 \cdot mol^{-1}$)
CO_2	7374	304.12	0.225	$9.395\,69 \times 10^{-5}$
N_2	3398	126.20	0.037	$8.924\,21 \times 10^{-5}$
CH_4	4599	190.56	0.011	$9.853\,05 \times 10^{-5}$
C_2H_6	4872	305.32	0.099	$1.453\,75 \times 10^{-4}$
C_3H_8	4248	369.83	0.152	$1.997\,85 \times 10^{-4}$
iC_4H_{10}	3650	408.20	0.183	$2.585\,00 \times 10^{-4}$
nC_4H_{10}	3796	425.12	0.200	$2.551\,36 \times 10^{-4}$
iC_5H_{12}	3390	460.40	0.227	$3.071\,43 \times 10^{-4}$
nC_5H_{12}	3370	469.70	0.252	$3.105\,71 \times 10^{-4}$
nC_6H_{14}	3025	507.60	0.300	$3.683\,29 \times 10^{-4}$
nC_7H_{16}	2740	540.20	0.350	$4.278\,39 \times 10^{-4}$

Information about the computer and operational system used in order to perform the calculations based on this paper, will be given in the next section.

4 Results and Discussion

Data for 44 mixtures are collected from thirteen literature sources. Their experimentally obtained critical temperatures and pressures are used to validate the method proposed in this paper. In order to fix the computation results and make them comparable, the values of the critical pressure (P_c), critical temperature (T_c), acentric factor (ω), and critical molar volume (v_c) for all of the pure components are shown in Table 1. Although the computation algorithm can also be applied to the condition corresponding to $k_{ij} = 0$, many researchers have found that the accuracy of any equation of state can be enhanced by using proper binary interaction coefficients [23,24]. Thus, this paper adopts the standard k_{ij} values of the PR and SRK EoS. The binary interaction coefficients for the PR EoS and the SRK EoS used in the paper are listed in Tables 2 and 3, respectively, [6].

The compositions of the 44 mixtures are listed in Table 4. The experimental data from the literature and the calculated results are shown in Table 5. In order to compare the proposed algorithm with at least one of the existing techniques, the commercial software package Calsep PVTSIM 20.0 was also used to calculate the critical points of the 44 mixtures. PVTSIM was developed by Calsep Co. in Denmark, and was specialized for the calculations of fluid properties. It has been widely used in oil and gas reservoir and flow assurance studies. Other commercial software, for example, SPT OLGA and PIPESIM, also use PVTSIM to generate the basic physical parameters [16].

The relative error (*RE*), the average absolute error (*AAE*), and the average relative error (*ARE*) are used to analyze the accuracy of the proposed method. The three errors are defined by

$$RE = \frac{x_{\mathrm{cal}i} - x_{\mathrm{exp}\,i}}{x_{\mathrm{exp\,i}}} \times 100\,\%, \tag{29}$$

Table 2 Binary interaction coefficients k_{ij} for the PR EoS

Component	CO_2	N_2	CH_4	C_2H_6	C_3H_8	iC_4H_{10}	nC_4H_{10}	iC_5H_{12}	nC_5H_{12}	nC_6H_{14}	nC_7H_{16}
CO_2	–	−0.019 9970	0.100 0000	0.129 8000	0.135 0000	0.129 8000	0.129 8000	0.125 0000	0.125 0000	0.125 0000	0.119 9000
N_2	−0.019 9970	–	0.035 9990	0.050 0000	0.079 9980	0.094 9990	0.090 0000	0.094 9990	0.100 0000	0.149 0000	0.143 9000
CH_4	0.100 0000	0.035 9990	–	0.002 2413	0.006 8288	0.013 1134	0.012 3047	0.017 6275	0.017 9254	0.023 4741	0.028 8643
C_2H_6	0.129 8000	0.050 0000	0.002 2413	–	0.001 2579	0.004 5736	0.004 0964	0.007 4133	0.007 6095	0.011 4138	0.015 3243
C_3H_8	0.135 0000	0.079 9980	0.006 8288	0.001 2579	–	0.001 0406	0.000 8189	0.002 5834	0.002 7005	0.005 1420	0.007 8874
iC_4H_{10}	0.129 8000	0.094 9990	0.013 1134	0.004 5736	0.001 0406	–	0.000 0133	0.000 3462	0.000 3900	0.001 5653	0.003 2212
nC_4H_{10}	0.129 8000	0.090 0000	0.012 3047	0.004 0964	0.000 8189	0.000 0133	–	0.000 4951	0.000 5472	0.001 8663	0.003 6464
iC_5H_{12}	0.125 0000	0.094 9990	0.017 6275	0.007 4133	0.002 5834	0.000 3462	0.000 4951	–	0.000 0013	0.000 4400	0.001 4592
nC_5H_{12}	0.125 0000	0.100 0000	0.017 9254	0.007 6095	0.002 7005	0.000 3900	0.000 5472	0.000 0013	–	0.000 3934	0.001 3733
nC_6H_{14}	0.125 0000	0.149 0000	0.023 4741	0.011 4138	0.005 1420	0.001 5653	0.001 8663	0.000 4400	0.000 3934	–	0.000 2972
nC_7H_{16}	0.119 9000	0.143 9000	0.028 8643	0.015 3243	0.007 8874	0.003 2212	0.003 6464	0.001 4592	0.001 3733	0.000 2972	–

Table 3 Binary interaction coefficients k_{ij} for the SRK EoS

Component	CO_2	N_2	CH_4	C_2H_6	C_3H_8	iC_4H_{10}	nC_4H_{10}	iC_5H_{12}	nC_5H_{12}	nC_6H_{14}	nC_7H_{16}
CO_2	–	−0.017 1000	0.095 6000	0.140 1000	0.136 8000	0.136 8000	0.141 2000	0.129 7000	0.134 7000	0.142 0000	0.109 2000
N_2	−0.017 1000	–	0.031 1990	0.031 8990	0.088 6000	0.131 5000	0.059 7000	0.093 0000	0.093 5980	0.165 0000	0.079 9890
CH_4	0.095 6000	0.031 1990	–	0.002 2413	0.006 8288	0.013 1134	0.012 3047	0.017 6275	0.017 9254	0.023 4741	0.028 8643
C_2H_6	0.140 1000	0.031 8990	0.002 2413	–	0.001 2579	0.004 5736	0.004 0964	0.007 4133	0.007 6095	0.011 4138	0.015 3243
C_3H_8	0.136 8000	0.088 6000	0.006 8288	0.001 2579	–	0.001 0406	0.000 8189	0.002 5834	0.002 7005	0.005 1420	0.007 8874
iC_4H_{10}	0.136 8000	0.131 5000	0.013 1134	0.004 5736	0.001 0406	–	0.000 0133	0.000 3462	0.000 3900	0.001 5653	0.003 2212
nC_4H_{10}	0.141 2000	0.059 7000	0.012 3047	0.004 0964	0.000 8189	0.000 0133	–	0.000 4951	0.000 5472	0.001 8663	0.003 6464
iC_5H_{12}	0.129 7000	0.093 0000	0.017 6275	0.007 4133	0.002 5834	0.000 3462	0.000 4951	–	0.000 0013	0.000 4400	0.001 4592
nC_5H_{12}	0.134 7000	0.093 5980	0.017 9254	0.007 6095	0.002 7005	0.000 3900	0.000 5472	0.000 0013	–	0.000 3934	0.001 3733
nC_6H_{14}	0.142 0000	0.165 0000	0.023 4741	0.011 4138	0.005 1420	0.001 5653	0.001 8663	0.000 4400	0.000 3934	–	0.000 2972
nC_7H_{16}	0.109 2000	0.079 9890	0.028 8643	0.015 3243	0.007 8874	0.003 2212	0.003 6464	0.001 4592	0.001 3733	0.000 2972	–

Table 4 Compositions of the studied multicomponent mixtures (in mole fractions)

Mix. no.	CO_2	N_2	CH_4	C_2H_6	C_3H_8	iC_4H_{10}	nC_4H_{10}	iC_5H_{12}	nC_5H_{12}	nC_6H_{14}	nC_7H_{16}
1			0.1	0.9							
2	0.95	0.05									
3				0.429			0.373				0.198
4				0.726			0.171				0.103
5				0.514			0.412				0.074
6				0.801				0.064			0.135
7				0.612				0.271			0.117
8				0.615				0.296			0.089
9		0.0465	0.453		0.5005						
10			0.193	0.47			0.337				
11			0.391	0.354			0.255				
12			0.04	0.821			0.139				
13			0.007	0.879			0.114				
14			0.461	0.443					0.095		
15			0.196	0.758					0.045		
16				0.996	0.001		0.003				
17				0.99	0.004		0.006				
18				0.98	0.016		0.004				
19				0.97	0.027		0.003				
20				0.3414	0.3421				0.3165		
21					0.3276		0.3398		0.3326		
22					0.201		0.399		0.4		
23					0.201		0.298		0.501		
24					0.198		0.106		0.696		
25							0.6449		0.2359	0.1192	
26			0.833	0.13	0.035						
27			0.8	0.039	0.161						
28		0.049	0.4345	0.0835	0.433						
29				0.6168			0.1376	0.0726			0.173
30				0.2542	0.2547		0.2554		0.2357		
31					0.4858		0.3316		0.1213	0.0613	
32		0.033	0.91	0.056	0.0012						
33		0.015	0.959	0.026	0.0001						
34		0.016	0.95	0.026	0.0078						
35				0.3977	0.2926		0.1997		0.0713	0.0369	
36			0.2019	0.2029	0.2033		0.2038		0.1881		
37		0.016	0.945	0.026	0.0081		0.0052				
38			0.1015	0.3573	0.2629		0.1794		0.0657	0.0332	
39		0.022	0.316	0.388	0.223		0.043		0.008		
40		0.014	0.943	0.027	0.0074		0.0049		0.001	0.0027	
41	0.0109	0.0884	0.8286	0.0401	0.0174	0.003	0.0055	0.0019	0.0012	0.0014	0.0006
42	0.002	0.24	0.7364	0.012	0.0053	0.001	0.0015	0.0005	0.0004	0.0004	0.0005
43	0.003	0.113	0.858	0.015	0.006	0.0012	0.0018	0.0006	0.0004	0.0004	0.0006
44	0.010	0.1611	0.7625	0.0369	0.016	0.0028	0.0051	0.0018	0.0011	0.0012	0.0015

$$AAE = \frac{1}{N}\sum_{i=1}^{N}\left|x_{\mathrm{cal}\,i} - x_{\mathrm{exp}\,i}\right|, \tag{30}$$

$$ARE = \frac{1}{N}\sum_{i=1}^{N}\frac{\left|x_{\mathrm{cal}\,i} - x_{\mathrm{exp}\,i}\right|}{x_{\mathrm{exp}_i}} \times 100\,\%, \tag{31}$$

Table 5 Critical parameters obtained from experiments, calculations based on this paper, and the PVTSIM software

Mix. no.	Number of components	Experimental		This paper SRK EoS		PVTSIM SRK EoS		This paper PR EoS		PVTSIM PR EoS		Data source
		T_c (K)	P_c (kPa)	T_c (K)	P_c (kPa)	T_c (K)	P_c (kPa)	T_c (K)	P_c(kPa)	T_c (K)	P_c (kPa)	
1	2	299	5322	299	5317	299	5325	299	5312	299	5319	[6]
2	2	302	8300	301	8075	301	8064	301	8060	300	8072	[25]
3	3	438	6612	442	6351	441	6607	439	6314	437	6309	[26]
4	3	386	7605	391	7558	391	7844	388	7462	387	7426	[26]
5	3	400	6405	405	6269	406	6393	404	6224	403	6200	[26]
6	3	391	8101	396	8383	396	8787	393	8262	391	8207	[26]
7	3	421	7156	423	7063	423	7237	420	7014	419	6968	[26]
8	3	416	7060	417	6924	417	7053	415	6875	414	6830	[26]
9	3	313	9232	323	9142	324	9064	321	9103	322	9033	[27]
10	3	354	7640	360	7301	361	7270	359	7263	359	7229	[28]
11	3	332	9720	338	9214	333	9214	336	9142	331	9131	[28]
12	3	324	5790	332	5902	333	5917	332	5872	332	5888	[28]
13	3	325	5480	329	5597	329	5617	329	5572	329	5593	[28]
14	3	311	10 340	310	10 280	311	10 277	308	10 129	309	10 124	[29]
15	3	311	6890	311	6845	312	6882	310	6791	311	6828	[29]
16	3	306	4900	306	4898	306	4911	306	4897	306	4909	[30]
17	3	307	4930	307	4927	307	4941	307	4925	307	4938	[30]
18	3	308	4960	308	4930	309	4987	308	4928	309	4983	[30]
19	3	309	4960	309	4939	309	4952	309	4936	309	4949	[30]
20	3	397	5600	405	5568	405	5564	404	5545	404	5541	[31]
21	3	429	4190	431	4174	429	4212	430	4168	429	4205	[31]
22	3	436	3850	439	3996	439	3998	439	3992	439	3993	[32]

Table 5 continued

Mix. no.	Number of components	Experimental		This paper SRK EoS		PVTSIM SRK EoS		This paper PR EoS		PVTSIM PR EoS		Data source
		T_c (K)	P_c (kPa)	T_c (K)	P_c (kPa)	T_c (K)	P_c (kPa)	T_c (K)	P_c(kPa)	T_c (K)	P_c (kPa)	
23	3	443	3900	444	3962	444	3963	444	3957	444	3959	[32]
24	3	449	3810	453	3863	453	3864	453	3860	453	3861	[32]
25	3	450	3880	451	3796	451	3793	450	3791	451	3787	[31]
26	3	228	6890	227	7009	227	7030	226	6962	227	6984	[33]
27	3	255	8960	251	9199	252	9200	250	9095	251	9098	[33]
28	4	313	8963	318	9029	318	8964	316	8987	316	8931	[27]
29	4	423	7412	426	7453	429	7769	423	7391	421	7357	[34]
30	4	406	5113	411	5073	411	5069	410	5060	411	5056	[31]
31	4	418	4506	420	4428	420	4428	419	4417	420	4416	[31]
32	4	199	5341	201	5490	201	5499	201	5480	201	5488	[35]
33	4	194	4932	196	5001	196	5006	195	4996	196	5000	[35]
34	4	197	5180	199	5301	199	5314	199	5290	199	5302	[35]
35	5	385	5620	389	5589	390	5589	388	5562	389	5562	[31]
36	5	387	7220	396	7062	396	7021	394	7040	394	6995	[31]
37	5	200	5456	202	5660	202	5680	202	5642	202	5663	[35]
38	6	376	6536	382	6478	383	6464	381	6444	381	6427	[31]
39	6	314	7846	319	7895	320	7878	318	7851	318	7834	[27]
40	7	201	5578	202	5829	202	5831	202	5846	202	5856	[35]
41	11	204	6584	204	6860	203	6804	204	6926	204	6966	[36]
42	11	183	5618	184	5986	–	–	183	6013	–	–	[36]
43	11	193	5829	193	5833	–	–	193	5842	–	–	[36]
44	11	198	6674	192	6450	–	–	193	6711	194	6763	[36]

Note: – represents that the PVTSIM software did not locate the critical points

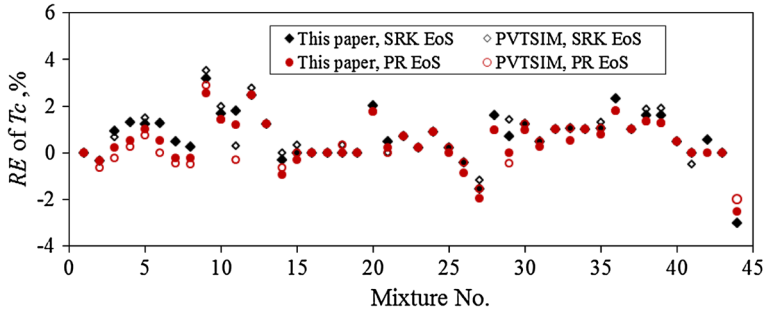

Fig. 3 *RE*s of calculated critical temperatures

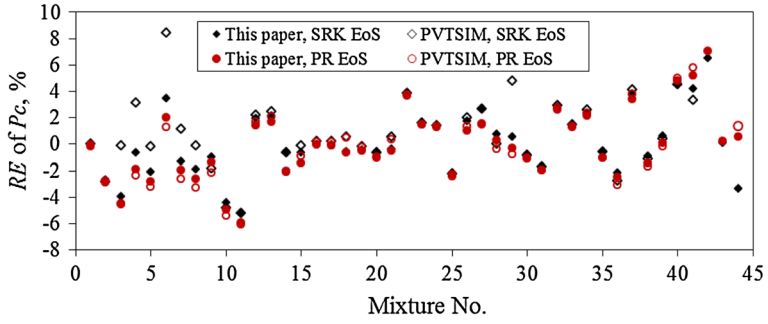

Fig. 4 *RE*s of calculated critical pressures

where x_{cal} is the calculated value, x_{exp} is the experimental value, subscript i is the index of the mixture number, and N is the number of studied mixtures, for which convergence could be reached.

*RE*s of the calculated critical temperatures and pressures are shown in Figs. 3 and 4.

The computer program additionally calculated the critical pressure and temperature of mixtures with more than 11 components. As there are almost no experimental data for mixtures with so many components, we decided to accomplish the main part of the validation based on mixtures that have up to 11 components. Thus, the *ARE*s are 0.948 % and 1.921 % regarding the critical temperature and critical pressure calculated with the proposed algorithm and SRK EoS, respectively, whereas the *ARE*s are 0.953 % and 1.968 % corresponding to the critical temperature and critical pressure calculated with the PTVSIM and based on the SRK EoS. Based on the PR EoS, the *ARE* is 0.768 % regarding the critical temperature and 1.992 % with regard to the critical pressure calculated with the proposed algorithm, whereas the *ARE* is 0.787 % for the critical temperature, and 2.080 % for the critical pressure calculated with the PTVSIM software package.

When the SRK EoS and the proposed damped Newton–Raphson algorithm are adopted, *AAE*s of critical-pressure and critical-temperature values are 123.82 kPa and 3.11 K, respectively. The *AAE*s based on the SRK EoS and the PVTSIM are 131.02 kPa and 3.24 K. When the PR EoS and the proposed algorithm are adopted, the two above

mentioned *AAE*s are 129.32 kPa and 2.45 K, whereas the *AAE*s based on the PVTSIM are 137.24 kPa and 2.55 K.

Many reasons contribute to these errors, for example, the error associated with the experimentally determined compositions of the mixtures, and the error associated with the measurement of the critical temperatures and pressures.

The comparisons show that when the same equations of state are adopted, the proposed algorithm has a higher accuracy than the PVTSIM software package. Besides, Table 5 shows that the PVTSIM software cannot always locate the liquid–vapor critical point even if there exists a critical point (Mix. No. 42, 43, 44 for the SRK EoS and No. 42, 43 for the PR EoS). For the above 44 mixtures listed in Table 4, all of the liquid–vapor critical points were successfully found by using the proposed damped Newton–Raphson algorithm.

The calculations based on this paper were performed by a 64-bit operating system, supported by Microsoft Visual Basic. The processor was an AMD A6-5400K (3.60 GHz). In addition, for a 43 component mixture, which is described in detail in [37] as fluid 2, convergence was reached in a total number of 21 iterations.

5 Conclusions

This paper proposes an improved Newton–Raphson method to calculate the liquid–vapor critical points of mixtures. The basic theoretical model is derived from the SRK EoS, PR EoS, and the rigorous definition of critical points. The model contains $C+2$ nonlinear equations and $C+2$ variables. By using the Newton–Raphson method, this model can be solved. However, the classical Newton–Raphson method may not converge successfully when it is applied to multicomponent mixtures. In order to eliminate this drawback, an improved damped Newton–Raphson method was developed and used, based on the existing Newton–Raphson method. The details regarding the improved convergence criteria, the adjustable damping coefficient, and finally, both the numerical and analytical derivatives of the Jacobian matrix are addressed. As a result, all equations and related conditions required for the computation of the scheme are illustrated in this paper. Finally, experimental data for the critical points of 44 mixtures are adopted in order to validate the method. The results show that the improved method can be used to compute liquid–vapor critical points of multicomponent mixtures in good agreement with reality.

Acknowledgments This paper is partly supported by the National Natural Science Foundation of China (No. 51174172), two sub-projects of the National Science and Technology Major Project of China (No. 2011ZX05054, No. 2011ZX05026-001-07), and a project of the Joint Research Fund for the Doctoral Program of Higher Education (No. 20125121110003).

Appendix 1

The general form of the cubic equation of state can be expressed by [5]

$$P = \frac{RT}{v-b} - \frac{a}{(v+D_1 b)\,(v+D_2 b)}. \tag{32}$$

Note: When the algorithm has converged successfully, Eq. 32 should be used to calculate the critical pressure as a function of the critical temperature, critical molar volume, and the corresponding EoS-dependent parameters. In this case, the thermodynamic variables shown in Eq. 32, have to be replaced by the critical ones.

Based on Eq. 32, the parameters in Eqs. 5 and 6 and thus indirectly in Eqs. 8 and 9 can be calculated as follows [11,13]:

$$\bar{N} = \sum_{i=1}^{C} \Delta n_i, \tag{33}$$

$$\alpha_k = \frac{\sum_{i=1}^{C} (y_i a_{ik})}{a}, \tag{34}$$

$$\bar{\alpha} = \sum_{i=1}^{C} (\Delta n_i \alpha_i), \tag{35}$$

$$\bar{a} = \frac{1}{a} \sum_{i=1}^{C} \sum_{j=1}^{C} \left(\Delta n_i \Delta n_j a_{ij}\right), \tag{36}$$

$$\beta_i = \frac{b_i}{b}, \tag{37}$$

$$\bar{\beta} = \sum_{i=1}^{C} (\Delta n_i \beta_i), \tag{38}$$

$$F_1 = \frac{1}{K-1}, \tag{39}$$

$$F_2 = \frac{2}{D_1 - D_2} \left[\frac{D_1}{K + D_1} - \frac{D_2}{K + D_2} \right], \tag{40}$$

$$F_3 = \frac{1}{D_1 - D_2} \left[\left(\frac{D_1}{K + D_1} \right)^2 - \left(\frac{D_2}{K + D_2} \right)^2 \right], \tag{41}$$

$$F_4 = \frac{1}{D_1 - D_2} \left[\left(\frac{D_1}{K + D_1} \right)^3 - \left(\frac{D_2}{K + D_2} \right)^3 \right], \tag{42}$$

$$F_5 = \frac{2}{D_1 - D_2} \ln \left(\frac{K + D_1}{K + D_2} \right), \tag{43}$$

$$F_6 = \frac{2}{D_1 - D_2} \left[\left(\frac{D_1}{K + D_1} - \frac{D_2}{K + D_2} \right) - \ln \left(\frac{K + D_1}{K + D_2} \right) \right], \tag{44}$$

$$K = \frac{v_c}{b}, \tag{45}$$

$$a = \sum_{i=1}^{C} \sum_{j=1}^{C} \left(\frac{n_i n_j}{n^2} a_{ij} \right), \tag{46}$$

$$b = \sum_{i=1}^{C} (y_i b_i), \tag{47}$$

$$a_{ij} = \left(a_i a_j\right)^{0.5} \left(1 - k_{ij}\right), \tag{48}$$

$$a_i = \frac{(RT_{ci})^2 \eta}{P_{ci}} \left[1 + c_i \left(1 - \left(\frac{T_c}{T_{ci}}\right)^{0.5}\right)\right]^2, \tag{49}$$

$$D_1 = \frac{u_0 + \sqrt{u_0^2 - 4w_0}}{2}, \tag{50}$$

$$D_2 = \frac{u_0 - \sqrt{u_0^2 - 4w_0}}{2}. \tag{51}$$

For the SRK EoS:

$$\eta = 0.42\,748,\ c_i = 0.48 + 1.574\omega_i - 0.176\omega_i^2,\ b_i = 0.08\,664\,RT_{ci}/P_{ci},\ u_0 = 1,\ w_0 = 0.$$

For the PR EoS:

$$\eta = 0.45\,724, \quad c_i = 0.37\,464 + 1.54\,226\omega_i - 0.26\,992\omega_i^2,$$
$$b_i = 0.07\,780RT_{ci}/P_{ci},\ u_0 = 2,\ w_0 = -1,$$

where T_c is the critical temperature of the mixture, v_c is the critical molar volume of the mixture, T_{ci} is the critical temperature of the ith component, P_{ci} is the critical pressure of the ith component, ω_i is the acentric factor of the ith component, k_{ij} is the binary interaction coefficient between the components i and j. The symbol of the universal gas constant is R.

Finally, n is the total number of moles that are in the mixture, as the sum of the individual component mole numbers n_i.

For calculations needing numerical partial differentiation in order to calculate the function derivatives appearing in the Jacobian matrix $\boldsymbol{J}$ in Eq. 12, the following notes are important.

In general, the approximations for the calculation of the numerical partial derivatives of the generalized functions ζ_i with respect to the generalized variables ξ_j (at constant ξ_l with $l \neq j$), are given by

$$\left(\frac{\partial \zeta_i}{\partial \xi_j}\right)_{\xi_l} \approx \frac{\zeta_i\left(\xi_1, \xi_2, \ldots, \xi_j + \Delta\xi_j, \ldots, \xi_u\right) - \zeta_i\left(\xi_1, \xi_2, \ldots, \xi_j, \ldots, \xi_u\right)}{\Delta\xi_j}, \tag{52}$$

where $u = C + 2$ for f_{1i} and f_2; $u = C$ for f_3.

$$\Delta\xi_j = 10^{-5}\xi_j \tag{53}$$

or in detail:

ζ_i each time represents the functions f_{1i}, f_2,and f_3. The variables $\xi_j$of both functions f_{1i} and f_2 are T_c, v_c and Δn_j, respectively, while f_3 depends only on the Δn_j-variables. In Eq. 52, a forward differencing has been shown, which in general is slightly less accurate than the calculation time-consuming centered differencing.

In many studies dealing with numerical differentiation, the coefficient 10^{-5} in Eq. 53 has been recommended as the optimum value for the minimization of the related numerical error. Heidemann and Khalil [10] also adopted this value.

Appendix 2

The derivatives appearing in the Jacobian matrix can alternatively be computed by using the following analytically derived expressions. It should be mentioned that although the whole expressions seem to make the computer program more complex, a further reduction of calculation time can be achieved, as the total number of computer calculations is reduced. We did all calculations with both numerical and analytical derivatives. We found that the results based on the analytical derivatives and, more specifically, with regard to the critical pressure, critical temperature, and the number of needed iteration steps are the same as those obtained from the computation of numerical derivatives, when those results are rounded down or rounded up to integers, with respect to the results in Table 5.

The partial derivatives of f_{1i}, f_2, and f_3 with respect to Δn_m are

$$\frac{\partial f_{1i}}{\partial(\Delta n_m)} = \frac{RT_c}{n}\left[\frac{1}{y_i}\frac{\partial(\Delta n_i)}{\partial(\Delta n_m)} + F_1\left(\beta_i\frac{\partial\bar{N}}{\partial(\Delta n_m)} + \frac{\partial\bar{\beta}}{\partial(\Delta n_m)}\right) + \beta_i F_1^2\frac{\partial\bar{\beta}}{\partial(\Delta n_m)}\right] + \frac{a}{bn}\left[\beta_i\frac{\partial\bar{\beta}}{\partial(\Delta n_m)}F_3 - \frac{F_5}{a}\sum_{j=1}^{C}\left(a_{ij}\frac{\partial(\Delta n_j)}{\partial(\Delta n_m)}\right) + F_6\left(\beta_i\frac{\partial\bar{\beta}}{\partial(\Delta n_m)} - \alpha_i\frac{\partial\bar{\beta}}{\partial(\Delta n_m)} - \beta_i\frac{\partial\bar{\alpha}}{\partial(\Delta n_m)}\right)\right], \tag{54}$$

$$\frac{\partial f_2}{\partial(\Delta n_m)} = \frac{RT_c}{n^2}\left[-\sum_{j=1}^{C}\frac{3\frac{\partial(\Delta n_j)}{\partial(\Delta n_m)}\Delta n_j^2}{y_j^2} + 3\frac{\partial\bar{N}}{\partial(\Delta n_m)}\left(\bar{\beta}F_1\right)^2 + 6\bar{N}\left(\bar{\beta}F_1\right)F_1\frac{\partial\bar{\beta}}{\partial(\Delta n_m)} + 6\left(F_1\bar{\beta}\right)^2F_1\frac{\partial\bar{\beta}}{\partial(\Delta n_m)}\right] + \frac{a\bar{\beta}}{n^2b}(F_3+F_6)\left[6\frac{\partial\bar{\beta}}{\partial(\Delta n_m)}\left(2\bar{\alpha}-\bar{\beta}\right) + 3\bar{\beta}\left(2\frac{\partial\bar{\alpha}}{\partial(\Delta n_m)} - \frac{\partial\bar{\beta}}{\partial(\Delta n_m)}\right)\right] - \frac{3a}{n^2b}\left[\frac{\partial\bar{\beta}}{\partial(\Delta n_m)}\left(\bar{a}F_6 + 2\bar{\beta}^2F_4\right) + \bar{\beta}F_6\frac{\partial\bar{a}}{\partial(\Delta n_m)}\right], \tag{55}$$

$$\frac{\partial f_3}{\partial(\Delta n_m)} = 2\Delta n_m, \tag{56}$$

where $i, m = 1, 2, \ldots, C$.

$$\frac{\partial(\Delta n_i)}{\partial(\Delta n_m)} = \delta_{im}. \tag{57}$$

Kronecker-Delta: $\delta_{im} = 1$ if $i = m$, otherwise is $\delta_{im} = 0$ (if $i \neq m$).

$$\frac{\partial(\Delta n_j)}{\partial(\Delta n_m)} = \delta_{jm}. \tag{58}$$

Kronecker-Delta: $\delta_{jm} = 1$ if $j = m$, otherwise is $\delta_{jm} = 0$ (if $j \neq m$).

$$\frac{\partial \bar{N}}{\partial(\Delta n_m)} = \delta_{mm} = 1, \tag{59}$$

$$\frac{\partial \bar{\beta}}{\partial(\Delta n_m)} = \beta_m, \tag{60}$$

$$\frac{\partial \bar{\alpha}}{\partial(\Delta n_m)} = \alpha_m, \tag{61}$$

$$\frac{\partial \bar{a}}{\partial(\Delta n_m)} = \frac{1}{a}\sum_{j=1}^{C}\left[\Delta n_j\left(a_{jm} + a_{mj}\right)\right]. \tag{62}$$

The partial derivatives of f_{1i} and f_2 with respect to v_c are

$$\frac{\partial f_{1i}}{\partial v_c} = \frac{RT_c}{n}\frac{\partial F_1}{\partial v_c}\left[\beta_i \bar{N} + \bar{\beta}\left(1 + 2\beta_i F_1\right)\right] + \frac{a}{bn}\left[\beta_i\bar{\beta}\frac{\partial F_3}{\partial v_c} - \frac{1}{a}\frac{\partial F_5}{\partial v_c}\sum_{j=1}^{C}\left(a_{ij}\Delta n_j\right) + \frac{\partial F_6}{\partial v_c}\left(\beta_i\bar{\beta} - \alpha_i\bar{\beta} - \bar{\alpha}\beta_i\right)\right] \tag{63}$$

$$\frac{\partial f_2}{\partial v_c} = 6\frac{RT_c F_1\bar{\beta}^2}{n^2}\frac{\partial F_1}{\partial v_c}\left(\bar{N} + \bar{\beta}F_1\right) + \frac{a\bar{\beta}}{n^2 b}\left[3\bar{\beta}\left(2\bar{\alpha} - \bar{\beta}\right)\left(\frac{\partial F_3}{\partial v_c} + \frac{\partial F_6}{\partial v_c}\right) - 2\bar{\beta}^2\frac{\partial F_4}{\partial v_c} - 3\bar{a}\frac{\partial F_6}{\partial v_c}\right], \tag{64}$$

where $i = 1, 2, \ldots, C$.

$$\frac{\partial F_1}{\partial v_c} = -\frac{1}{b\left(K-1\right)^2}, \tag{65}$$

$$\frac{\partial F_3}{\partial v_c} = \frac{2}{b\left(D_1 - D_2\right)}\left[\frac{D_2^2}{\left(K + D_2\right)^3} - \frac{D_1^2}{\left(K + D_1\right)^3}\right], \tag{66}$$

$$\frac{\partial F_4}{\partial v_c} = \frac{3}{b\left(D_1 - D_2\right)}\left[\frac{D_2^3}{\left(K + D_2\right)^4} - \frac{D_1^3}{\left(K + D_1\right)^4}\right], \tag{67}$$

$$\frac{\partial F_5}{\partial v_c} = \frac{-2}{b\left(K + D_1\right)\left(K + D_2\right)}, \tag{68}$$

$$\frac{\partial F_6}{\partial v_c} = \frac{2}{D_1 - D_2}\left[\frac{D_2}{b\left(K + D_2\right)^2} - \frac{D_1}{b\left(K + D_1\right)^2} - \frac{D_2 - D_1}{b\left(K + D_1\right)\left(K + D_2\right)}\right]. \tag{69}$$

The partial derivatives of f_{1i} and f_2 with respect to T_c are

$$\begin{aligned}\frac{\partial f_{1i}}{\partial T_c} &= \frac{R}{n}\left[\frac{\Delta n_i}{y_i} + F_1\left(\beta_i \bar{N} + \bar{\beta}\right) + \beta_i F_1^2 \bar{\beta}\right] \\ &\quad + \frac{1}{bn}\frac{\partial a}{\partial T_c}\left[\beta_i \bar{\beta} F_3 + F_6\left(\beta_i \bar{\beta} - \alpha_i \bar{\beta} - \bar{\alpha}\beta_i\right)\right] \\ &\quad - \frac{aF_6}{bn}\left(\bar{\beta}\frac{\partial \alpha_i}{\partial T_c} + \beta_i \frac{\partial \bar{\alpha}}{\partial T_c}\right) - \frac{F_5}{bn}\sum_{j=1}^{C}\left(\Delta n_j \frac{\partial a_{ij}}{\partial T_c}\right), \end{aligned} \tag{70}$$

$$\begin{aligned}\frac{\partial f_2}{\partial T_c} &= \frac{R}{n^2}\left[-\sum_{j=1}^{C}\frac{\Delta n_j^3}{y_j^2} + 3\bar{N}\left(\bar{\beta}F_1\right)^2 + 2\left(F_1\bar{\beta}\right)^3\right] \\ &\quad + \frac{\bar{\beta}}{n^2 b}\frac{\partial a}{\partial T_c}\left[3\bar{\beta}\left(2\bar{\alpha} - \bar{\beta}\right)\left(F_3 + F_6\right) - 2\bar{\beta}^2 F_4 - 3\bar{a}F_6\right] \\ &\quad + \frac{3\bar{\beta}a}{n^2 b}\left[2\bar{\beta}\left(F_3 + F_6\right)\frac{\partial \bar{\alpha}}{\partial T_c} - F_6\frac{\partial \bar{a}}{\partial T_c}\right], \end{aligned} \tag{71}$$

where $i = 1, 2, \ldots, C$.

$$\begin{aligned}\frac{\partial a_{ij}}{\partial T_c} &= -\frac{\left(1 - k_{ij}\right)R^2 T_{ci} T_{cj}\eta}{\sqrt{P_{ci}P_{cj}}}\left\{\frac{c_i}{2\sqrt{T_c T_{ci}}}\left[1 + c_j\left(1 - \sqrt{\frac{T_c}{T_{cj}}}\right)\right]\right. \\ &\quad \left. + \frac{c_j}{2\sqrt{T_c T_{cj}}}\left[1 + c_i\left(1 - \sqrt{\frac{T_c}{T_{ci}}}\right)\right]\right\}, \end{aligned} \tag{72}$$

$$\begin{aligned}\frac{\partial a_{ki}}{\partial T_c} &= -\frac{\left(1 - k_{ki}\right)R^2 T_{ck} T_{ci}\eta}{\sqrt{P_{ck}P_{ci}}}\left\{\frac{c_k}{2\sqrt{T_c T_{ck}}}\left[1 + c_i\left(1 - \sqrt{\frac{T_c}{T_{ci}}}\right)\right]\right. \\ &\quad \left. + \frac{c_i}{2\sqrt{T_c T_{ci}}}\left[1 + c_k\left(1 - \sqrt{\frac{T_c}{T_{ck}}}\right)\right]\right\}, \end{aligned} \tag{73}$$

$$\begin{aligned}\frac{\partial a_{kj}}{\partial T_c} &= -\frac{\left(1 - k_{kj}\right)R^2 T_{ck} T_{cj}\eta}{\sqrt{P_{ck}P_{cj}}}\left\{\frac{c_k}{2\sqrt{T_c T_{ck}}}\left[1 + c_j\left(1 - \sqrt{\frac{T_c}{T_{cj}}}\right)\right]\right. \\ &\quad \left. + \frac{c_j}{2\sqrt{T_c T_{cj}}}\left[1 + c_k\left(1 - \sqrt{\frac{T_c}{T_{ck}}}\right)\right]\right\}, \end{aligned} \tag{74}$$

$$\frac{\partial a}{\partial T_c} = \sum_{k=1}^{C}\sum_{j=1}^{C}\left(\frac{n_k n_j}{n^2}\frac{\partial a_{kj}}{\partial T_c}\right), \tag{75}$$

$$\frac{\partial \bar{a}}{\partial T_c} = -\frac{1}{a^2}\frac{\partial a}{\partial T_c}\sum_{k=1}^{C}\sum_{j=1}^{C}\left(\Delta n_k \Delta n_j a_{kj}\right) + \frac{1}{a}\sum_{k=1}^{C}\sum_{j=1}^{C}\left(\Delta n_k \Delta n_j \frac{\partial a_{kj}}{\partial T_c}\right), \tag{76}$$

$$\frac{\partial \alpha_i}{\partial T_c} = \frac{1}{a^2}\left[a\sum_{k=1}^{C}\left(y_k\frac{\partial a_{ki}}{\partial T_c}\right) - \frac{\partial a}{\partial T_c}\sum_{k=1}^{C}\left(y_k a_{ki}\right)\right], \tag{77}$$

$$\frac{\partial \alpha_j}{\partial T_c} = \frac{1}{a^2}\left[a\sum_{k=1}^{C}\left(y_k\frac{\partial a_{kj}}{\partial T_c}\right) - \frac{\partial a}{\partial T_c}\sum_{k=1}^{C}\left(y_k a_{kj}\right)\right], \tag{78}$$

$$\frac{\partial \bar{\alpha}}{\partial T_c} = \sum_{j=1}^{C}\left(\Delta n_j\frac{\partial \alpha_j}{\partial T_c}\right). \tag{79}$$

A note regarding the binary interaction coefficients k_{ij}: For k_{ij} with $i \neq j$, the binary interaction coefficients shown in Tables 2 and 3 have been used. The value 0 has been used for any binary interaction coefficient k_{ij} with $i = j$ (in other words: $k_{ii} = k_{jj} = 0$).

A note with regard to the universal gas constant: computational value, $R = 8.3145\,\mathrm{J{\cdot}mol^{-1}{\cdot}K^{-1}}$.

References

1. S. Mokhatab, W.A. Poe, *Handbook of Natural Gas Transmission and Processing* (Elsevier, Amsterdam, 2012), http://www.sciencedirect.com/science/book/9780123869142
2. W. Jia, C. Li, Z. Li, *Pipelines* (ASCE, Fortworth, TX, 2013), p. 1501
3. J. Sengers, Int. J. Thermophys. **6**, 203 (1985)
4. C. Li, X. Wu, W. Jia, K. Liu, K. Liao, *International Oil and Gas Conference and Exhibition in China* (SPE, Beijing, 2010)
5. A. Danesh, *PVT and Phase Behaviour of Petroleum Reservoir Fluids* (Elsevier, Amsterdam, 1998), http://www.sciencedirect.com/science/bookseries/03767361/47
6. API, *API Technical Data Book*, 7th edn. (Epcon International, Houston, 2005)
7. M.L. Michelsen, Fluid Phase Equilib. **4**, 1 (1980)
8. D.O. Ortiz-Vega, D.E. Cristancho, K.R. Hall, G.A. Iglesias-Silva, Ind. Eng. Chem. Res. **50**, 97 (2010)
9. G. Venkatarathnam, Ind. Eng. Chem. Res. **53**, 3723 (2014)
10. R.A. Heidemann, A.M. Khalil, AlChE J. **26**, 769 (1980)
11. W. Jia, C. Li, X. Wu, Int. J. Thermodyn. **15**, 149 (2012)
12. M.C. Wang, D.S.H. Wong, H. Chen, W. Yan, T.-M. Guo, Chem. Eng. Sci. **54**, 3873 (1999)
13. B.A. Stradi, J.F. Brennecke, P. Kohn, M.A. Stadtherr, AlChE J. **47**, 212 (2001)
14. D.N. Justo-García, F. García-Sánchez, J. Águila-Hernández, R. Eustaquio-Rincón, Fluid Phase Equilib. **264**, 164 (2008)
15. N.I. Henderson, W.F. Sacco, N.E. Barufatti, M. Ali, Ind. Eng. Chem. Res. **49**, 1872 (2010)
16. C. Hussen, R. Amin, G. Madden, B. Evans, J. Nat. Gas Sci. Eng. **5**, 42 (2012)
17. B.P. Flannery, S.A. Teukolsky, W.T. Vetterling, *Numerical Recipes in C: The Art of Scientific Computing (Fortran Version)* (Cambridge University Press, London, 1995)
18. R.E. Bank, D.J. Rose, Numer. Math. **37**, 279 (1981)
19. P.T. Harker, J.-S. Pang, Lect. Appl. Math. **26**, 265 (1990)
20. R. Rannacher, *Einführung in die Numerische Mathematik: (Numerik 0); Vorlesungsskriptum SS 2005* (Institut für Angewandte Mathematik, Heidelberg, 2006)
21. P. Deuflhard, *Newton Methods for Nonlinear Problems: Affine Invariance and Adaptive Algorithms, Springer Series in Computational Mathematics*, vol. 35 (Springer, Berlin, 2011)
22. T. Rung, L. Xue, J. Yan, *Vorlesungsskript* (Technische Universität Berlin, HFI, 2001)
23. J.-N. Jaubert, F. Mutelet, Fluid Phase Equilib. **224**, 285 (2004)
24. R. Privat, J.-N. Jaubert, in *Thermodynamic Models for the Prediction of Petroleum-Fluid Phase Behaviour*, chap. 5, ed. by M.E. Abdel-Raouf. Crude Oil Emulsions-Composition Stability and Characterization (InTech, Rijeka, Croatia, 2012)

25. P.N. Seevam, J.M. Race, M.J. Downie, J. Pipe Eng. **6**, 133 (2007)
26. E. Brunner, J. Chem. Thermodyn. **22**, 335 (1990)
27. L. Yarborough, L. Smith, SPE J. **10**, 298 (1970)
28. H.M. Cota, G. Thodos, J. Chem. Eng. Data **7**, 62 (1962)
29. R.R. Spear, R.L. Robinson Jr, K.-C. Chao, Ind. Eng. Chem. Fundam. **10**, 588 (1971)
30. P. Uchytil, I. Wichterle, Fluid Phase Equilib. **15**, 209 (1983)
31. D.O. Etter, W.B. Kay, J. Chem. Eng. Data **6**, 409 (1961)
32. J.M. Nelson, D.E. Holcomb, Chem. Eng. Prog., Symp. Ser. **49**, 93–106 (1953)
33. A.R. Price, R. Kobayashi, J. Chem. Eng. Data **4**, 40 (1959)
34. O. Ekiner, G. Thodos, J. Chem. Eng. Data **11**, 457 (1966)
35. F. Farshchi Tabrizi, K. Nasrifar, J. Nat. Gas Sci. Eng. **2**, 21 (2010)
36. P. Davis, A. Bertuzzi, T. Gore, F. Kurata, J. Pet. Technol. **6**, 37 (1954)
37. F. García-Sánchez, J.L. Ruiz-Cortina, C. Lira-Galeana, L. Ponce-Ramírez, Fluid Phase Equilib. **81**, 39 (1992)